IgG and IgM glycosylation patterns in patients undergoing image-guided tumor ablation

Lucas D. Breen, Maja Pučić-Baković, Frano Vučković, Karli Reiding, Irena Trbojević-Akmačić, Martina Šrajer Gajdošik, Madeleine I. Cook, Michael J. Lopez, Manfred Wuhrer, L.M. Camara, Uroš Andjelković, Damian E. Dupuy, Djuro Josić

PII: S0304-4165(16)00020-9
DOI: doi: 10.1016/j.bbagen.2016.01.011
Reference: BBAGEN 28369

To appear in: *BBA - General Subjects*

Received date: 13 November 2015
Accepted date: 1 January 2016

Please cite this article as: Lucas D. Breen, Maja Pučić-Baković, Frano Vučković, Karli Reiding, Irena Trbojević-Akmačić, Martina Šrajer Gajdošik, Madeleine I. Cook, Michael J. Lopez, Manfred Wuhrer, L.M. Camara, Uroš Andjelković, Damian E. Dupuy, Djuro Josić, IgG and IgM glycosylation patterns in patients undergoing image-guided tumor ablation, *BBA - General Subjects* (2016), doi: 10.1016/j.bbagen.2016.01.011

IgG and IgM glycosylation patterns in patients undergoing image-guided tumor ablation

Lucas D. Breen[1], Maja Pučić-Baković[2] , Frano Vučković[2], Karli Reiding[3], Irena Trbojević-Akmačić[2], Martina Šrajer Gajdošik[1*], Madeleine I. Cook[6], Michael J. Lopez[4], Manfred Wuhrer[3,5], L. M. Camara[6], Uroš Andjelković[7], Damian E. Dupuy[6], Djuro Josić[7,8]

[1]Proteomics Core, COBRE CCRD, Rhode Island Hospital, Providence, RI, USA

[2]Genos Ltd., Glycobiology Research Laboratory, Zagreb, Croatia

[3]Leiden University Medical Center, Center for Proteomics and Metabolomics, Leiden, The Netherlands

[4]Center for Statistical Sciences, Brown University, Providence, RI, USA

[5]VU University Amsterdam, Division of BioAnalytical Chemistry, Amsterdam, The Netherlands

[6]Department of Diagnostic Imaging, Warren Alpert Medical School, Brown University, Providence, RI, USA

[7]Department of Biotechnology, University of Rijeka, Croatia

[8]Department of Medicine, Warren Alpert Medical School, Brown University, Providence, RI, USA

Corresponding Authors:
Djuro Josic, PhD
Department of Biotechnology, University of Rijeka, Radmile Matejcic 2, 51000 Rijeka, Croatia
Phone: +385 51 701 415
Fax: +385-51-406-588
E-mail: Djuro_Josic@brown.edu

Damian E. Dupuy, M.D.
Department of Diagnostic Imaging, Rhode Island Hospital, Alpert Medical School at Brown University, 593 Eddy Street, Providence, RI 02903
Phone: 401-444-5184
Fax: 401-444-5017
E-mail: DDupuy@Lifespan.org

*Present address: Department of Chemistry, J. J. Strossmayer University, 31000 Osijek, Croatia

Abstract

Background: Image-guided tumor ablation is a technique whereby needle-like applicators are placed directly into solid tumors under guidance typically with computed tomography or ultrasound. Changes in IgG and IgM antibody glycosylation were studied during ablation-induced immune response to cancer, and the use of glycosylation as a biomarker for diagnosis, prognosis and disease treatment was examined.

Methods: Plasma from 27 tumor patients was collected immediately before, after and for 6 months following ablation. IgG and IgM antibodies were isolated by use high-throughput chromatography, and analyzed by hydrophilic liquid chromatography. Thorough identification of glycan structures in each chromatography peak was performed by nano-liquid chromatography electrospray ionization mass spectrometry.

Results: Although antibody glycosylation was found to vary with cancer type, discernable patterns of change based on the successful treatment of tumors by ablation were not identified. One patient with renal clear cell carcinoma and poor disease outcome had unexpectedly high amount of oligomannose IgG glycans during the whole period of monitoring. In contrast, IgM antibodies did not follow the same pattern.

Conclusions: These findings suggest that glycosylation patterns are indicative of an immune system that is unable to prevent different types of cancer, rather than products of the immunostimulatory response to the ablation of tumor itself. Analyses of the outcome effect suggested that IgG and IgM glycosylation are not associated with tumor ablation.

General Significance: Present work opens a new way for parallel determination of glycosylation changes of both IgG and IgM antibodies by use of high-throughput methods, and their future use as biomarkers for disease diagnosis and prognosis.

Keywords: Tumor ablation, IgG, IgM, glycosylation

1. Introduction

Image-guided tumor ablation (IGTA) is a technique whereby needle-like applicators are placed directly into solid tumors under guidance typically with computed tomography (CT) or ultrasound. The applicators can deliver cytotoxic heat with radiofrequency or microwave energy, or cytotoxic cold with pressurized argon gas [1]. IGTA has become increasingly utilized to treat tumors in the liver, lung and kidney because of its minimal invasiveness [2-4]. Little is known about the underlying host response after a cancerous tumor has been destroyed *in situ* by these techniques. Humoral immunity is thought to be an important component of IGTA function [4, 5], of which IgG and IgM are a major part [6-8]. It is hypothesized that aggressive in-situ tumor ablation combined with immunotherapy may release tumor-specific antigens and enhance immunological response resulting in the destruction of residual primary tumor and metastases [4, 6-8]. However, most investigations have been carried out on cell culture [6, 9, 10] and animal models [2, 6, 9], and little clinical data is available [4, 8, 11].

Immunoglobulins are glycoproteins and have covalently attached N-glycans at specific N-glycosylation sites. Microheterogeneity in the attached N-glycan can profoundly change their effector function [12-16]. Disease-associated changes in IgG glycosylation were first described almost three decades ago. The first abnormality of this kind was identified in rheumatoid arthritis (RA) patients, who present with a very high rate of IgG glycans lacking two terminal galactoses (IgG-G0) [14, 17, 18]. Abnormally high levels of IgG-G0 have also been reported in liver fibrosis/cirrhosis [19], pancreatitis, pancreatic adenocarcinoma [20] and ovarian cancer [21], and have been associated with increased rates of metastasis in prostate [22], gastric and lung cancers [23].

In this study, we aimed to gain a better understanding of IgG and IgM antibody-based immune response to cancer by identifying glycosylation patterns that may be specific to different cancer types and we tracked these changes in glycosylation patterns in response to IGTA. For this sake, in addition to already developed method for the analysis of IgG glycosylation by hydrophilic liquid chromatography, we

developed and applied the same approach to thoroughly analyze IgM glycosylation patterns. Parallel, high-throughput determination of IgG and IgM glycosylation patterns opens the way for their use as potential diagnostic and prognostic biomarkers, and possibly gives an additional platform for post-ablation treatment of certain cancer patients.

2. Materials and Methods

2.1. Plasma Collection

Plasma was collected from 9 control individuals (age 57-81, mean 65.7) and 27 patients (age 57-85, average 70.3) undergoing ablation therapy for liver, renal and lung tumors. Blood samples from patients were collected in heparinized tubes immediately before ablation, and then subsequently after 1 hour, 4 hours, 1 week, 2 weeks, 1 month, 3 months, and 6 months.

Samples were screened to exclude the presence of blood-borne viruses (hepatitis A, B and C, and HIV) and plasma was isolated from cellular components via centrifugation. Patients included in this study had neoplasms over 2 cm in size, laboratory values of granulocytes ≥ 1,500/μL and platelet count ≥ 75,000/μL. This prospective study was approved by the institutional review board and was compliant with the Health Insurance Portability and Accountability Act (HIPAA, Rhode Island Hospital, Providence, RI, USA). All patients signed a study-specific informed consent form. General patient clinical information is found in **Table 1**.

2.2. Clinical Information

In total, our data include 8 liver cancer patients, 6 lung cancer patients, and 13 renal cancer patients. One patient underwent two liver tumor ablations, data from which was split into two halves such that each ablation could be analyzed separately by longitudinal analysis. The specific pathology of each tumor was obtained via biopsy, or from the best judgment of the physician performing the ablation when biopsy was not an option.

The clinical outcome of each patient was determined under the direction of the physician, broadly generalized into “good” or “poor” outcomes. “Good” outcome was

indicated for patients who were successfully treated and had no appreciable disease following ablation, or who had a successful ablation but experienced a decline in health for unrelated issues. A distinction of "poor" outcome was given to patients who had residual tumor, tumor progression or metastasis following ablation (**Table 1**).

2.3. Chemicals

Chemicals for buffer preparations (phosphate buffered saline (PBS), tris, hydrochloric acid, sodium chloride, sodium hydroxide, ammonium bicarbonate, citric acid, Igepal CA-630, sodium dodecyl sulfate, formic acid (FA), acetonitrile (ACNACN), ethanol and 2-aminobenzamide (2-AB), 2-picoline borane (2-PB), dimethyl sulfoxide) were purchased from Fisher Scientific (Pittsburgh, PA, USA) and Sigma-Aldrich (St. Louis, MO, USA). Ultra-pure water was used throughout.

2.4. IgG and IgM Isolation

Successful isolation of high-purity IgG and IgM was achieved by sequential separation of human plasma using Protein A chromatography followed by QA (quaternary amine) strong anion exchange chromatography as previously described in detail [24]. Briefly, for initial separation of immunoglobulins from plasma, glass columns with an inner diameter of 6.5 mm packed with 1 mL of Toyopearl AF-rProtein A-650F support (Tosoh Bioscience, Stuttgart, Germany) were used. Concentrated and desalted Protein A eluate was subsequently applied to the 0.34 mL CIM QA Disk Monolithic Columns (BIA Separations, Ajdovscina, Slovenia) and the unbound fraction containing IgG was collected. The bound fraction was eluted by a step gradient with 0.225 M NaCl to remove contaminating proteins and with 0.5 M NaCl to finally elute IgM.

Concentration of IgG in collected fractions was evaluated via Bicinchoninic Acid Protein Assay kit (Pierce, Thermo Scientific, Rockford, IL, USA) according to the manufacturer's procedure. The concentration of IgM inthe collected fractions was determined by quantitative evaluation of scanned bands following IgM specific immunoblot as described previously [24].

For subsequent glycan analysis, desalting of IgG and IgM fractions was performed. IgG fractions were applied to a Protein A column and washed with 5 column

volumes of water before being eluted with 0.1 M FA and being adjusted to pH 7.4 using 1 M ammonium bicarbonate. IgM fractions were desalted by gel filtration using PD-10 desalting columns (GE Healthcare, Uppsala, Sweden) according to the manufacturer's procedure.

2.5. Glycan Release and Labeling

IgG and IgM glycan release and labeling was performed as reported previously [25]. Briefly, isolated immunoglobulins were denatured with 2% SDS (*w/v*) and by incubation at 65 °C for 10 min. Subsequently, 4% (v/v) Igepal CA-630 non-ionic detergent was added to the mixture, and N-glycans were released with the addition of N-glycosidase F (ProZyme, San Leandro, CA, USA) in PBS and overnight incubation at 37 °C. Released N-glycans were fluorescently labeled by reductive amination with 2-AB as fluorescent dye, and 2-PB as reductant by 2 hours incubation at 65 °C. Labeled N-glycans were then purified from free label and reducing agent by hydrophilic interaction liquid chromatography solid phase extraction (HILIC-SPE).

2.6. Hydrophilic Interaction Chromatography of IgG and IgM N-Glycans

Fluorescently labeled N-glycans were separated by hydrophilic interaction on a Waters Acquity ultra performance liquid chromatography (UPLC) instrument containing of a quaternary solvent manager, sample manager and a FLR fluorescence detector set with excitation and emission wavelengths of 330 and 420 nm respectively. The instrument was under the control of Empower 3 software (Waters, Milford, MA, USA). Labeled N-glycans were separated on a Waters BEH glycan chromatography column, 100 x 2.1 mm i.d., 1.7 µm BEH particles, with 100 mM ammonium formate, pH 4.4, as solvent A and ACN as solvent B. The separation method for IgG N-glycans used a linear gradient of 75-62 % ACN (*v/v*) at flow rate 0.4 ml/min in a 25 min analytical run. The separation method for IgM N-glycans used a linear gradient of 75-60 % ACN (*v/v*) at flow rate 0.4 mL/min in a 30 min analytical run. Samples were maintained at 5 °C before injection, and the separation temperature at 60 °C for both separation methods. Glycan profiles were calibrated against a dextran ladder prepared from hydrolyzed and 2-AB labeled glucose oligomers. Data processing was performed using an automatic processing method

with a traditional integration algorithm after which each chromatogram was manually corrected in order to maintain the same intervals of integration for all samples. IgG and IgM chromatograms were separated into 24 and 32 peaks respectively, and the abundance of each chromatographic peak was expressed as a percent of the total integrated area.

2.7. Identification of IgG and IgM N-glycan structures

The identity of IgG N-glycans eluting in each chromatography peak had previously been determined by exoglycosidase digestion and mass spectrometry [26]. Since this is the first time that the Waters BEH chromatography column was used for separation of IgM N-glycans, the same approach was applied for identification of IgM N-glycans released from pooled healthy human plasma IgM. Preliminary identification was performed by exoglycosidase digestions in conjunction with hydrophilic interaction chromatography. Identities of glycans were confirmed via mass spectrometry following initial chromatographic separations. 2-AB labeled glycan fractions were dried down by vacuum centrifugation, re-suspended in water and analyzed by nano-LC-ESI-MS/MS. Chromatographic separation was performed on an Ultimate 3000 RSLCnano system (Dionex/Thermo Scientific, Sunnyvale, CA) equipped with a 100 µm x 2 cm Acclaim Pepmap 100 trap column (C18, 100 Å pore size, 5 µm particle size) and a 75 µm x 15 cm Acclaim Pepmap RSLC column (C18, 100 Å pore size, 2 µm particle size) (both from Thermo Scientific, Etten-Leur, The Netherlands). Solvents used were 0.1% FA as solvent A and 95% ACN as solvent B. The columns were equilibrated at a flow rate of 500 µL/min with solvent A for 5 min, after which the sample was loaded. Elution was performed as a linear gradient, starting at 0% solvent B to 25% solvent B in 15 min, followed by a 5 min gradient to 70% solvent B. This concentration was maintained for another 5 min, after which the column was brought to 0% solvent B in 1 min. Washing was performed with another 24 min of 0% solvent B. All steps were performed at 32°C. The LC system was coupled to an AmaZon ESI-IT-MS (Bruker Daltonics, Bremen, Germany) operated in the positive ion mode, using a nanospray source at 4500 V and performing evaporation at 250 °C with a dry gas flow of 5 L/min. Ions from *m/z* 500 to 1600 were registered. Automatic fragment ion analysis of the five most abundant

ions resulted in MS/MS spectra in a detection window of *m/z* 140 to 2200. Glycan structures were assigned using GlycoWorkbench [27]. Lists of all IgG and IgM N-glycan structures identified in chromatography peaks are available as **Supplementary Tables 1** and **2**, respectively.

2.8. Derived Glycosylation Traits

The total incidence of the following glycosylation traits was derived from the relative abundance of 24 IgG or 32 IgM chromatography peaks: fucosylation, bisecting *N*-acetylglucosamine (GlcNAc), galactosylation (0, 1 or 2 residues), sialylation (0, 1 or 2 residues), prevalence of sialylation of galactose residues and prevalence of oligomannose glycans. Only the most abundant glycan structure in each peak was taken into account. Formulas used in calculation of derived glycosylation traits are provided as **Supplementary Table 3**.

2.9. Statistical Analysis

Association analysis between glycosylation traits and tumor location was performed using analysis of covariance model (ANCOVA) with age and sex included as additional covariates.

Longitudinal analysis of patient samples through their six month observation period was performed by implementing a linear mixed effects model controlled for age, sex and tumor location (modeled as fixed effects) and individual (modeled as random effect).

To investigate association between patient clinical outcome and derived glycosylation traits, an ANCOVA model was utilized. Ablation outcome was defined as “good” or “poor” as described earlier. Two models were used, one adjusted for age and sex, and the second adjusted for age, sex and tumor location.

Prior to the analyses, glycan variables were all transformed to standard Normal distribution by inverse transformation of ranks to Normality (R package "GenABEL", function rntransform). Using rank transformed variables makes estimated effects of different glycans comparable as these will have the same standardized variance. False discovery rate (FDR) was controlled by the Benjamini-Hochberg procedure at the specified level of 0.05.

3. Results

3.1. IgG and IgM glycoprofiling

In this study plasma was collected from 27 patients undergoing ablation therapy for liver, renal and lung tumors and 9 healthy controls (**Table 1**). Plasma from patients was collected before ablation and at seven time points during the following six months. IgG was isolated from the plasma by affinity chromatography using Toyopearl Protein A support followed by further purification through strong anion exchange chromatography using CIM QA monolithic columns. After collecting the IgG fraction, IgM was eluted from the QA column in a two-step elution system. N-glycans were enzymatically released from the isolated Igs, fluorescently labeled, and analyzed by HILIC. HILIC-UPLC profiles of IgG glycans were obtained for the entire study cohort. As for the lesser abundant IgM, glycan profiles with peak intensities above S/N of 10 were obtained for 11 patients (4 liver, 4 lung and 3 renal tumors) and 3 controls.

Examples of obtained IgG and IgM glycan profiles are given in **Figure 1** and **2**, respectively, with the most abundant glycans indicated for each chromatography peak. Identities of the glycans found on IgG and IgM were assigned based on their established elution properties, registered *m/z* and fragmentation spectra, and are available as **Supplementary Tables 1** and **2**, respectively. Normal polyclonal human IgG N-glycans are known to be mostly biantennary complex-type structures which are heavily core-fucosylated and may contain bisecting GlcNAc and/or sialic acid [12, 17]. We were able to identify a total of 33 IgG N-glycan structures: 30 complex, 1 oligomannose and 2 hybrid N-glycans. In our normal IgG N-glycan pool the most abundant structures were: FA2 (GP4), FA2G1 (GP8 and 9), FA2G2 (GP14) and FA2G2S1 (GP18) (**Figure 1**).

Normal human IgM is predominantly occupied with core-fucosylated biantennary structures which are, compared to IgG, more sialylated and bisected [12, 28, 29]. Next to this higher level of complexity, IgM is also known to contain a high level of

oligomannose N-glycans [29]. In this study we have identified a total of 42 IgM N-glycan structures: 29 complex, 5 oligomannose and 8 hybrid N-glycans. The most abundant structures found in our normal IgM N-glycan pool were: M6 (GP12), FA2G2S1 (GP25), FA2BG2S1 (GP26) and FA2BG2S2 (GP32) (**Figure 2**).

Tumor	Ablation type[1]	Age	Gender	Pathology[2]	Outcome (generalized)
Liver	MW	57.92	Male	HCC	Good
	RFA	58.43	Male	HCC	Poor
	MW	64.57	Male	HCC	Poor
	MW	68.74	Male	colorectal cancer (metastatic)	Poor
	MW	70.32	Female	cholangiocarcinoma	Poor
	RFA	70.32	Male	highly suspicious for HCC	Poor
	MW	71.00	Female	HCC	Poor
	MW	84.82	Male	HCC	Poor
Lung	RFA	56.78	Male	nonsmall cell lung cancer, adenocarcinoma	Good

Table 1. General patient characteristics within the clinical cohort.

				status post partial chemoradiation	
	RFA	72.92	Female	adenocarcinoma	Good
	MW	73.74	Male	squamous cell carcinoma (metastatic)	Poor
	MW	79.24	Female	carcinoid	Good
	MW	84.35	Female	adenocarcinoma	Good
	MW	85.27	Male	squamous cell carcinoma	Good
Renal	RFA	56.63	Male	papillary RCC	Good
	MW	57.51	Male	clear cell RCC (metastatic)	Poor
	RFA	60.05	Male	non-diagnostic histology, likely papillary RCC	Good
	RFA	62.25	Female	Unknown (looked like clear cell RCC)	Good
	MW	64.82	Male	highly suspicious for RCC	Good
	RFA	67.47	Male	papillary RCC	Good
	RFA	68.67	Male	clear cell RCC	Good
	RFA	69.33	Male	clear cell RCC	Good
	RFA	70.50	Male	clear cell RCC	Good
	RFA	74.09	Male	clear cell RCC	Poor
	RFA	80.07	Male	clear cell RCC	Good
	RFA	83.44	Female	papillary RCC	Good
	RFA	83.57	Male	clear cell RCC	Good

[1] RFA - radiofrequency ablation; MW - microwave ablation

[2] RCC - renal cell carcinoma; HCC - hepatocellular carcinoma

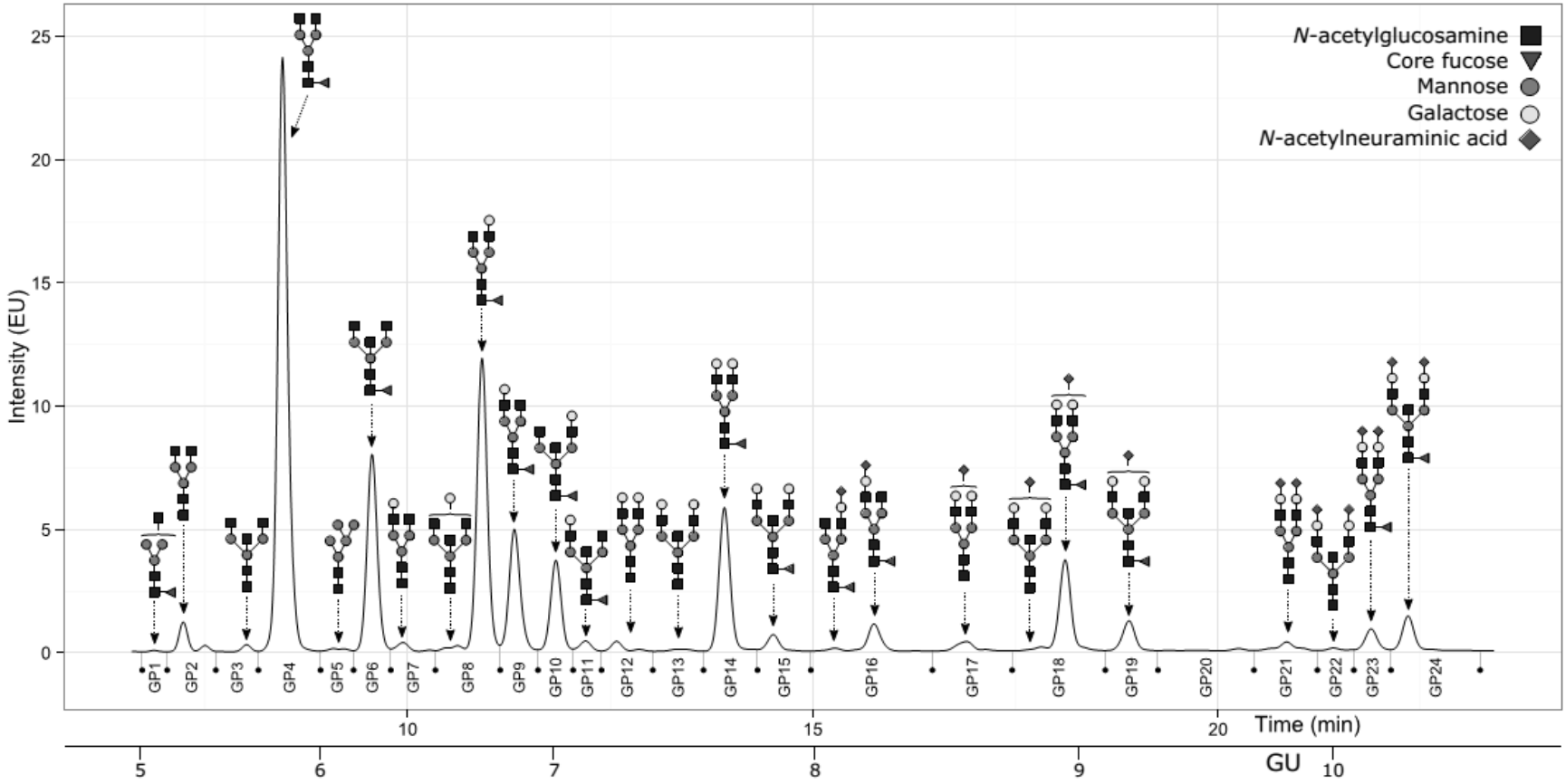

Figure 1. Representative example of a chromatogram obtained by HILIC-UPLC analysis of IgG N-glycans of a healthy person. Only the most abundant N-glycans in each chromatography peak are shown. For a full list of detected IgG N-glycans see Supplementary Table 1. Glycan schemes are given in terms of: square (N-acetylglucosamine), triangle (fucose), dark circle (mannose), light circle (galactose), and diamond (N-acetylneuraminic acid).

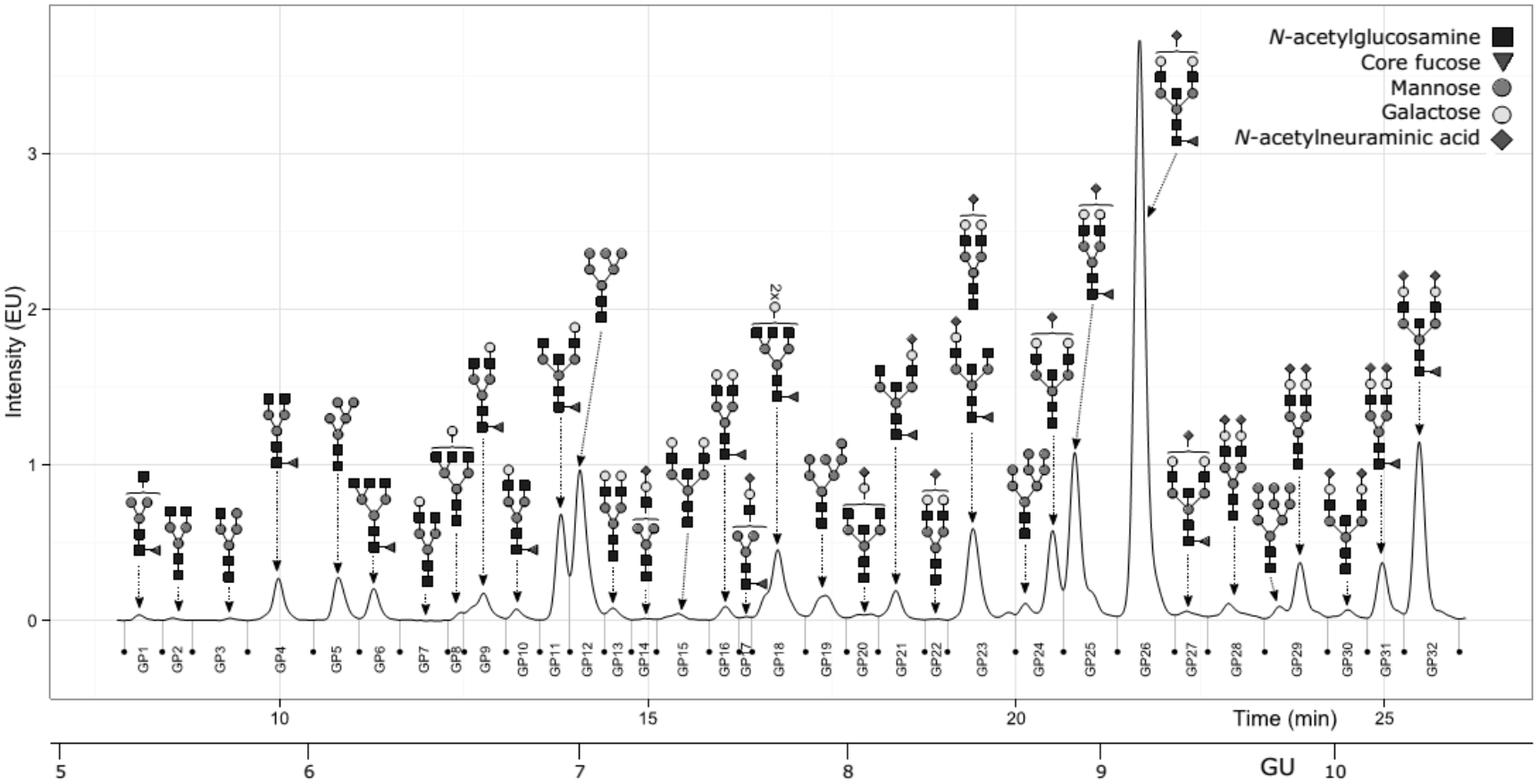

Figure 2. Representative example of a chromatogram obtained by HILIC-UPLC analysis of IgM N-glycans. Only the most abundant N-glycans in each chromatography peak are shown. For a full list of detected IgM N-glycans see Supplementary Table 2. Glycan schemes are given as in Figure 1.

3.2. Changes in IgG glycosylation

The prevalence of different IgG glycosylation traits (e.g. galactosylation, sialylation, fucosylation) was compared between controls and patients before tumor ablation using ANCOVA model. Descriptives and association analysis results for derived IgG glycosylation traits are available as **Tables 2 and 3**, respectively.

Patients suffering from liver tumor showed the most pronounced differences compared to controls (**Figure 3**). With increase in the prevalence of agalactosylated glycans (G0; 44% vs 27%, $p = 1x10^{-4}$) and decrease in monogalactosylated (G1; 32% vs 40%, $p = 2x10^{-4}$) and digalactosylated glycans (G2; 24% vs 34%, $p = 4x10^{-4}$), IgG galactosylation of liver tumor patients was found to be significantly lower than in controls (**Tables 2** and **3**).

A similar trend was observed in lung and renal tumor, although statistical significance was obtained only for decrease in G1 glycans (35% vs 40%, $p = 2x10^{-2}$) in lung tumor and for increase in G0 glycans (33% vs 27%, $p = 5x10^{-2}$) in renal tumor patients (**Tables 2** and **3**).

Pronounced differences were found in the relative abundance of sialylated glycans in liver and lung tumor patients. When compared to controls, lower levels of monosialylated glycans (S1; 11% vs 13%, $p = 4x10^{-4}$) were revealed for liver tumor patients (**Tables 2** and **3**). Quite the opposite was observed for lung tumor where levels of disialylated glycans (S2; 5% vs 4%, $p = 3x10^{-2}$) were higher than in controls (**Tables 2** and **3**). Because all sialic acid residues must build on galactose residues, another possibility to look at this is to look at the prevalence of galactose residues that are sialylated (S/G; see **Supplementary Table 3** for calculation). This allows us to remove the bias in sialylation levels that is introduced by differing levels of galactosylation among patient groups. When examining this, we noticed a significant difference between controls and patients, with liver and lung tumor patients appearing higher than controls (liver 28% vs 21%, $p = 8x10^{-4}$; lung 26% vs 21%, $p = 1x10^{-2}$; **Tables 2** and **3**).

With regard to the prevalence of core-fucosylated glycans (F) and glycans with bisecting GlcNAc (B), no significant differences were detected between patients and controls (**Table 2** and **3**).

Only one oligomannose N-glycan, M5, was detected in the IgG glycan pool. When the level of this glycan was compared between tumor patients and controls, again we could not observe any difference.

Among renal tumor patients, 8 patients were identified as clear cell renal cell carcinoma (RCC), 4 were identified as papillary RCC, and the pathology of one patient was undetermined. There were a number of IgG glycosylation traits in which papillary RCC patients showed significant differences compared to clear cell RCC, especially in disialylated glycans (data not shown). Papillary RCC patients had higher prevalence of disialylated glycans ($p \leq 7x10^{-3}$) and lower core-fucosylation ($p = 5x10^{-3}$) than clear cell RCC patients.

Collection of patient samples before ablation and throughout six months observation after ablation allowed the longitudinal analysis of IgG glycosylation. Longitudinal linear mixed effects analysis indicated that none of the glycosylation traits shows significant change over the time (data not shown). The time-series graphs are shown in **Supplementary Figure 1.**

During the clinical trial the outcome of the patient was broadly generalized into "good" or "poor" categories. Association between patient clinical outcome and derived IgG glycosylation traits was examined with an ANCOVA model, adjusted for age and sex, which indicated an effect of galactosylation on patient outcome (data not shown). However, when tumor location was added as a covariate into the model, no significant difference in IgG glycosylation profiles between patients with different clinical outcome was evident anymore (**Table 5**).

Table 2. Descriptive statistics of derived IgG and IgM glycosylation traits for tumor patients and controls. Median and interquartile range (in parenthesis) shown. G0 – the prevalence of agalactosylated glycans, G1 – the prevalence of monogalactosylated glycans, G2 - the prevalence of digalactosylated glycans, F – the prevalence of core-fucosylated glycans, B - the prevalence of glycans with bisecting *N*-acetylglucosamine, S0 - the prevalence of asialylated glycans, S1 – the prevalence of monosialylated glycans, S2 - the prevalence of disialylated glycans, S/G - the prevalence of sialylation of galactosylated glycans, and OM - the prevalence of oligomannose glycans.

Derived glycosylation trait	IgG				IgM			
	Control	Liver tumor	Lung tumor	Renal tumor	Control	Liver tumor	Lung tumor	Renal tumor
G0	27.31 (3.90)	43.83 (6.41)	29.48 (11.47)	32.76 (9.63)	2.27 (0.71)	4.20 (0.93)	3.71 (0.54)	2.89 (0.68)
G1	39.59 (2.32)	32.04 (8.63)	34.61 (4.41)	36.36 (4.46)	6.94 (1.35)	10.01 (2.42)	7.90 (0.91)	8.34 (0.68)
G2	33.70 (4.52)	24.10 (2.97)	35.86 (6.38)	30.39 (5.16)	74.52 (3.02)	65.18 (8.88)	69.61 (3.39)	72.17 (3.13)
F	94.11 (2.10)	94.76 (1.73)	93.97 (2.20)	94.70 (2.63)	69.16 (2.21)	63.33 (8.13)	67.34 (2.83)	69.28 (4.21)
B	20.12 (2.69)	22.34 (4.18)	20.59 (2.95)	21.20 (1.14)	44.23 (1.37)	46.94 (1.01)	44.46 (1.62)	46.31 (0.81)
S0	83.33 (2.34)	85.40 (2.20)	77.81 (4.75)	83.30 (1.81)	26.27 (3.58)	34.29 (4.09)	31.03 (2.16)	28.36 (3.22)
S1	12.99 (1.57)	10.92 (0.50)	15.49 (3.71)	13.14 (1.80)	54.76 (1.16)	52.68 (4.08)	53.47 (1.24)	55.86 (2.51)
S2	3.56 (1.23)	3.29 (1.51)	4.89 (1.53)	3.45 (1.27)	19.16 (3.39)	13.05 (3.76)	16.56 (1.45)	15.79 (5.73)
S/G	20.97 (2.81)	27.73 (3.93)	25.54 (8.73)	24.04 (4.40)	61.60 (2.84)	56.64 (4.95)	60.08 (1.74)	58.52 (5.29)
OM	0.33 (0.13)	0.39 (0.08)	0.40 (0.27)	0.32 (0.17)	12.36 (0.85)	15.01 (3.72)	12.21 (1.26)	11.52 (1.13)

Table 3. Association analysis between derived IgG glycosylation traits and tumor location. Significant values are in bold and indicate that the value of a certain derived glycosylation trait is significantly different between controls and tumor patients. Description of derived glycosylation traits as in Table 2.

Derived glycosylation trait	Liver tumor			Lung tumor			Renal tumor		
	effect	**SE**	**p.adj**	**effect**	**SE**	**p.adj**	**effect**	**SE**	**p.adj**
G0	1,980	0,336	**9,8E-05**	0,866	0,453	8,21E-02	0,855	0,366	**5,00E-02**
G1	-1,817	0,334	**1,54E-04**	-1,121	0,385	**1,79E-02**	-0,510	0,403	2,46E-01
G2	-1,606	0,337	**3,62E-04**	-0,550	0,446	2,43E-01	-0,826	0,416	8,02E-02
F	0,432	0,398	3,15E-01	-0,202	0,550	7,52E-01	0,068	0,563	9,31E-01
B	1,086	0,636	1,17E-01	0,219	0,556	7,45E-01	0,491	0,335	1,78E-01
S0	0,629	0,376	1,20E-01	-0,268	0,465	6,08E-01	0,290	0,499	6,20E-01
S1	-1,245	0,263	**3,62E-04**	0,097	0,493	8,61E-01	-0,542	0,480	3,07E-01
S2	0,885	0,484	9,98E-02	1,122	0,440	**3,42E-02**	0,473	0,485	3,81E-01
S/G	1,809	0,411	**7,53E-04**	1,390	0,455	**1,33E-02**	0,843	0,416	7,65E-02
OM	0,492	0,336	1,74E-01	0,899	0,516	1,09E-01	0,437	0,534	4,72E-01

SE - standard error

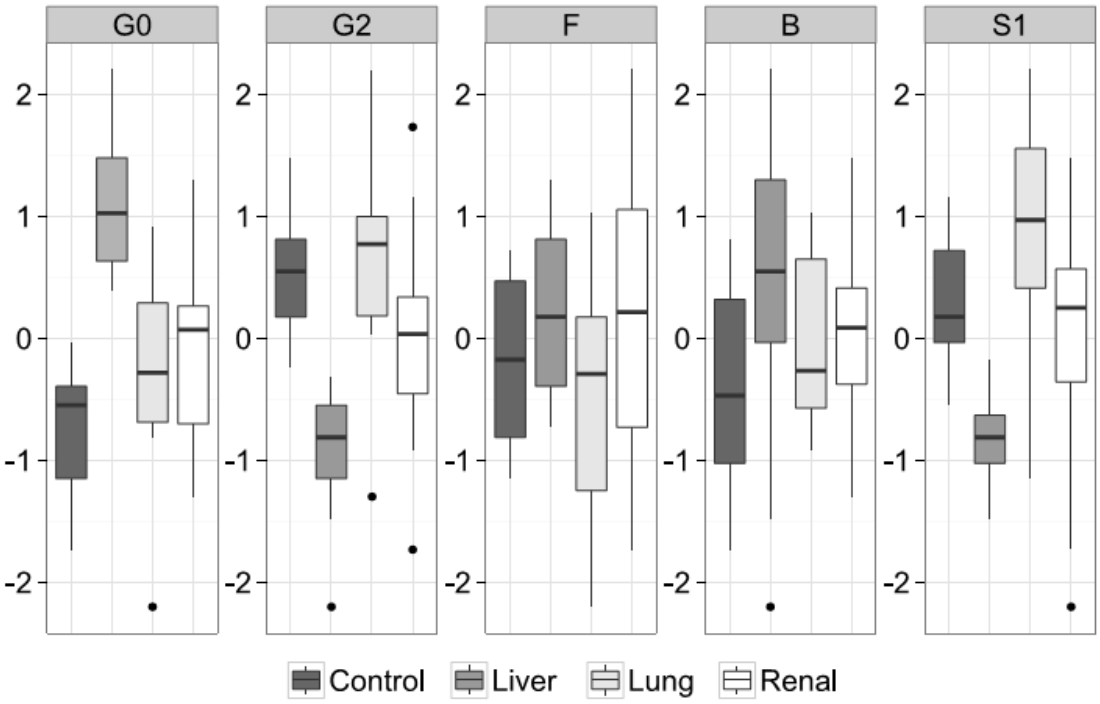

Figure 3. Comparison of derived IgG glycosylation traits of controls and tumor (liver, lung and renal) patients before ablation. G0 – the prevalence of agalactosylated glycans, G2 - the prevalence of digalactosylated glycans, F – the prevalence of core-fucosylated glycans, B - the prevalence of glycans with bisecting N-acetylglucosamine, and S1 – the prevalence of monosialylated glycans. Standardized values of derived glycosylation traits on y-axis.

3.3. Changes in IgM glycosylation

As with IgG we have analyzed association between IgM glycosylation traits and tumor location. Descriptives and association analysis results for derived IgM glycosylation traits are available as **Tables 2** and **4**, respectively. A statistically significant difference in derived IgM glycosylation traits between patients and controls was only detected in liver tumor (**Table 4**). Similar to IgG, liver tumor patients showed lower galactosylation of IgM glycans than controls (**Figure 4**). This was seen from both higher prevalence G0 (4% vs 2%, $p = 4x10^{-2}$) and G1 glycans (10% vs 7%, $p = 2x10^{-2}$) as well as from lower prevalence of G2 glycans (65% vs 75%, $p = 5x10^{-2}$; **Tables 2** and **4**). All other derived IgM glycosylation traits (prevalence of core-fucose, bisecting GlcNAc, sialic acids and oligomannose glycans) in liver tumor patients did not show any significant difference from controls.

Although there was no difference in derived glycosylation traits between lung and renal tumor patients and controls, we did see some change in single IgM glycan peaks. Compared to controls, lung tumor patients had slightly lower level of the most abundant IgM glycan peak GP26 (FA2BG2S1), while renal tumor patients had an increase in relatively low abundant glycan peak GP21 (FA2[6]BG1S1; for peaks see **Figure 2**).

As with our IgG data, no obvious time-related trends in IgM glycosylation traits were apparent during six months observation period (data not shown). The time-series graphs for IgM data are shown in **Supplementary Figure 1.**

Similar to the longitudinal analysis results, no significant difference in IgM glycosylation profiles between patients with different clinical outcome was revealed (**Table 5**).

Table 4. Association analysis between derived IgM glycosylation traits and tumor location. Significant values are in bold and indicate that the value of a certain derived glycosylation trait is significantly different between controls and tumor patients. Description of derived glycosylation traits as in Table 2.

Derived glycosylation trait	Liver tumor			Lung tumor			Renal tumor		
	effect	**SE**	**p.adj**	**effect**	**SE**	**p.adj**	**effect**	**SE**	**p.adj**
G0	1,333	0,416	**3,56E-02**	1,057	0,859	2,43E-01	0,054	1,056	9,45E-01
G1	2,027	0,542	**1,66E-02**	0,852	1,064	4,34E-01	0,532	0,730	5,36E-01
G2	-2,017	0,681	**4,80E-02**	-0,835	1,051	4,34E-01	-0,495	0,781	5,78E-01
F	-0,808	0,857	4,34E-01	0,272	0,587	6,39E-01	0,136	0,748	8,96E-01
B	1,228	0,887	2,49E-01	0,464	0,440	2,78E-01	1,036	0,472	8,08E-02
S0	1,524	0,902	1,87E-01	0,466	1,364	7,12E-01	-0,194	1,069	8,96E-01
S1	-0,852	0,670	2,78E-01	-0,717	0,795	3,62E-01	-0,943	1,029	4,33E-01
S2	-1,213	0,857	2,49E-01	0,097	0,783	9,03E-01	0,507	0,984	6,39E-01
S/G	-0,871	0,781	3,43E-01	0,401	1,082	6,89E-01	0,539	1,031	6,39E-01
OM	0,622	0,745	5,06E-01	-0,857	0,589	1,87E-01	-1,117	0,906	2,63E-01

SE - standard error

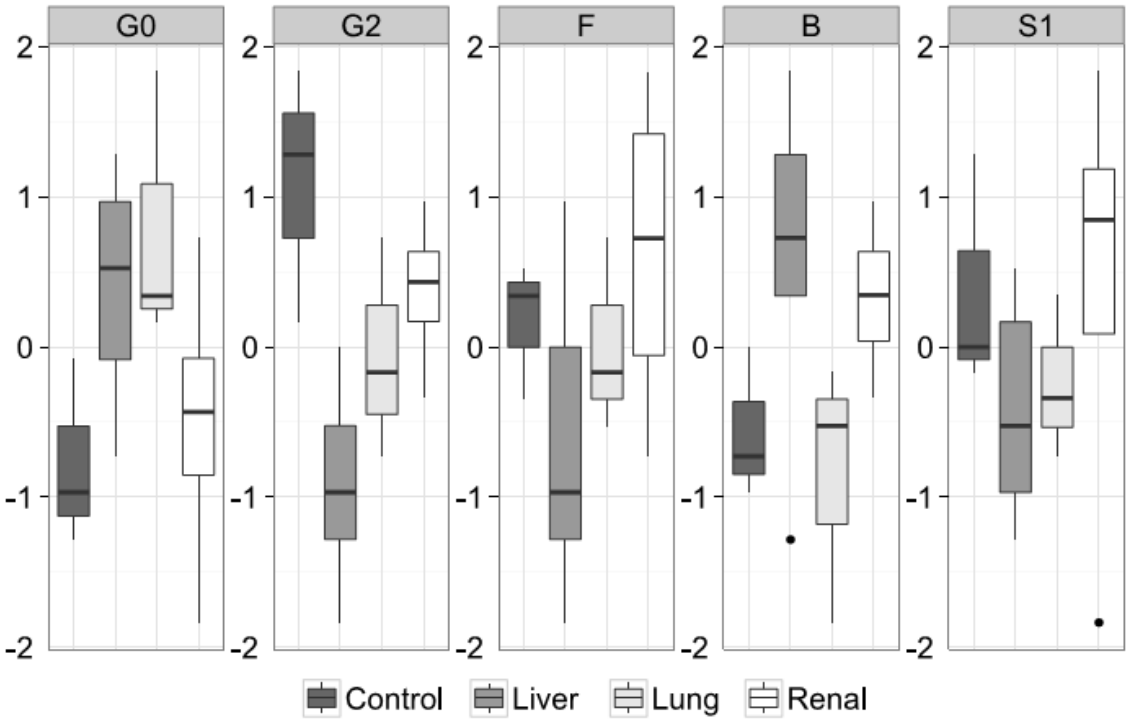

Figure 4. Comparison of derived IgM glycosylation traits of controls and tumor (liver, lung and renal) patients before ablation. Description of derived glycosylation traits as in Table 2. Standardized values of derived glycosylation traits on y-axis.

Table 5. Association analysis between patient clinical outcome and derived IgG and IgM glycosylation traits. Description of derived glycosylation traits as in Table 2.

Derived glycosylation trait	IgG			IgM		
	effect	SE	p.adj	effect	SE	p.adj
G0	-0,488	0,446	7,35E-01	0,914	0,651	3,24E-01
G1	0,269	0,434	8,02E-01	-0,340	0,542	5,47E-01
G2	0,627	0,470	6,93E-01	0,602	0,569	5,05E-01
F	-0,127	0,573	8,02E-01	1,138	0,732	3,24E-01
B	-0,232	0,559	8,02E-01	-0,007	0,813	9,91E-01
S0	-0,354	0,500	8,02E-01	-0,367	0,514	5,38E-01
S1	0,197	0,499	8,02E-01	0,707	0,851	5,05E-01
S2	0,691	0,480	6,93E-01	0,157	0,749	8,52E-01
S/G	0,113	0,492	8,02E-01	-0,403	0,725	5,47E-01
OM	-0,395	0,546	8,02E-01	-0,507	0,590	5,05E-01

SE - standard error

3.4. Unexpected IgG glycosylation case

During the course of this study an unusual IgG N-glycan profile was observed for one of the renal tumor patients initially included in the study (the patient was excluded from statistical analysis). This 70 year old male was diagnosed with clear cell RCC and additionally an ITP disorder, resulting in "poor" clinical outcome. As shown in **Figure 5**, his composition of IgG glycans was vastly different from all other patients and controls. The most prominent difference were unusually high abundances of oligomannose N-glycans (identified by exoglycosidase digestion with Jack bean α-mannosidase). These oligomannose N-glycans (M5, M6, M7, M8 and M9) are generally of very low abundance on IgG (< 1% of total IgG glycan pool) but their abundance for this patient before ablation and during the following six months averaged 15%. In addition, compared to other patients we noticed higher abundance of a complex FA2BG2S1 glycan (GP19; 12% vs 2%) and lower abundance (on average two-fold) of less complex biantennary IgG N-glycans with none or one galactose (FA2, FA2G1). In contrast to the IgG glycosylation data, no such extreme difference in oligomannose N-glycans was observed for IgM (data not shown). However, as with IgG, the IgM of the patient contained higher abundance of FA2BG2S1 glycan (GP26; 35% vs 27%) and in general lower abundance (on average two-fold) of less complex biantennary IgM N-glycans with one or two galactoses.

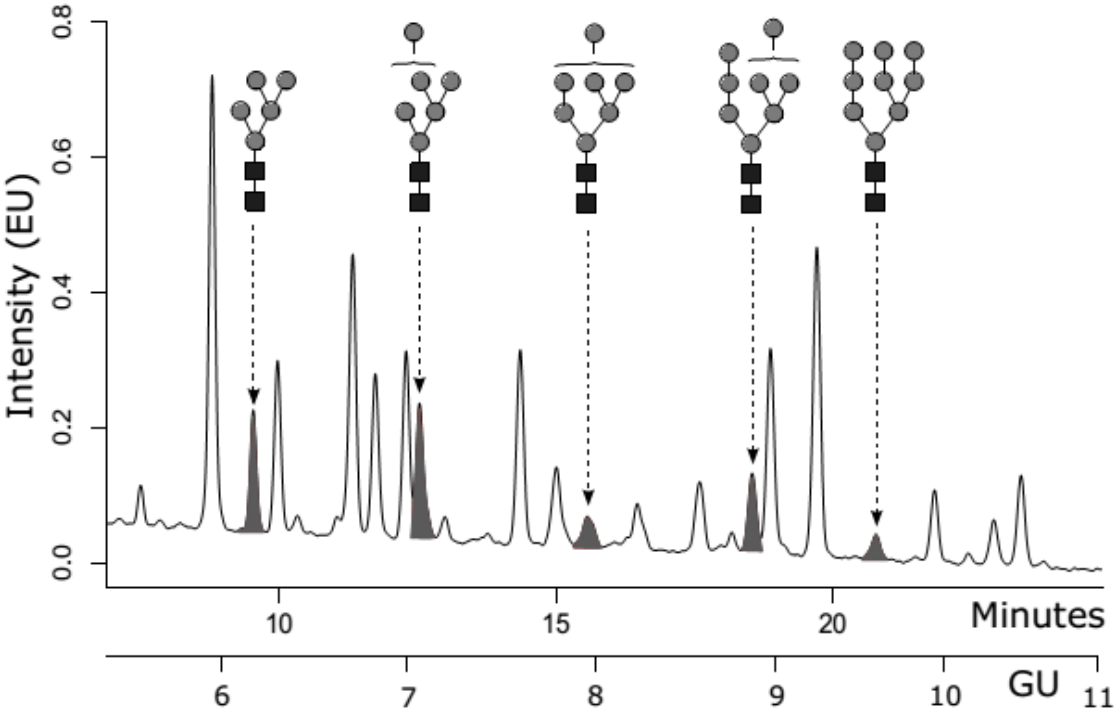

Figure 5. IgG N-glycan profile of renal tumor patient with unexpectedly high abundant oligomannose N-glycans

4. Discussion

The use of different methods for image-guided tumor ablation (mostly thermal) is expanding due to new technical developments and the minimal side effects involved [1-4]. The potential secondary advantage of the *in situ* destruction of malignant tissue is the immunologic response resulting in the potential generation of an anti-tumor immune response. This response may be triggered by the immune-assisted absorption and degradation of the destroyed malignant tissue [4-6, 8]. There are some case reports that describe spontaneous regression of some tumors after ablation, which may indicate possible involvement of the immune system [2, 5, 8]. Additional research suggests that ablation has a stimulatory effect in this process [5, 6]. Some studies also demonstrate that the tumor ablation may modulate the immune system and both immunostimulatory and immunosuppressive responses may be triggered [2, 4, 8, 9].

Guided by the above mentioned discussion about possible involvement of the immune system in destruction of tumor tissue after ablation [2, 5, 8], we took a closer look at IgG and IgM concentrations following ablation. However, no significant change in concentration of IgG and IgM in the monitored period was found [24]. Therefore, an extensive investigation of the glycosylation profiles of isolated patient IgG and IgM antibodies was initiated using a recently developed high-throughput method [26]. During sample accrual an extensive proteomic investigation was also initiated. However, only a minor increase in concentration of inflammatory proteins could be found [24, 30].

Human IgG contains an N-linked glycosylation site at the Asn297 residue on each of its heavy chains within the Fc region. At their core, the glycan structures that occupy these positions are biantennary heptasaccharides composed of *N*-acetylglucosamine (GlcNAc) and mannose. Large amounts of variation are seen within the sugar residues attached to this core structure, often containing mixtures of GlcNAc, galactose, core fucose and terminal sialic acid [12, 13]. Depending largely on the glycosylation patterns of the Fc region, IgG can initiate antibody-dependent cell-mediated cytotoxicity (ADCC) or complement-dependent cytotoxicity (CDC) [13,

14]. Additional residues on this glycan structure can confer additional effects, for example, addition of terminal sialic acid to the glycan chain of IgG converts its effector function from inflammatory to an anti-inflammatory effect [15, 16, 31]. High doses of intravenous polyclonal IgG (IVIG) collected from the plasma of large groups of healthy donors is currently used for therapy of immunodeficient patients, and for the treatment of autoimmune diseases such as idiopathic thrombocytopemic purpura (ITP) and Kawasaki's disease. The mechanism of IVIG therapeutic activity is still topic of intense discussion, but it seems clear that its glycosylated Fc is responsible for some of the activities [31, 32].

IgM is the second most abundant immunoglobulin in human plasma, and the first immunoglobulin produced in primary immune response. IgM largely recognizes multiple antigens with low affinity, but IgM induced by antigen exposure is characterized by much higher antigen specificity. The polymeric structure and consequent polyreactivity of this immunoglobulin is one of the key properties that enable its different functions [12, 33]. Human IgM has five glycosylation sites on each heavy chain located at Asn-171, Asn-332, Asn-395, Asn-402 and Asn-563, and additionally a single glycosylation site on J chain. [12, 34]. Unlike antigen-bound IgG, antigen-bound IgM pentamers do not activate the complement system via the MBL pathway [12, 33, 35]. This fact seems to play an important role in the rather limited use of concentrates of purified human IgM for antigen replacement therapy [32, 36, 37]. It has been recently shown that glycosylation, and especially sialylation, of IgM has an important role in function of this antibody [28], again making IgM replacement therapy a discussion point [29, 32, 38, 39].

Glycosylation analysis illustrated that among pre-ablation samples, the incidence of IgG-G0 in liver cancer patients was higher, and also renal and lung ablation patients presented slightly elevated IgG-G0 levels compared to controls. As high amounts of IgG-G0 have been associated with liver fibrosis and cirrhosis [19], part of the trend seen in our patients with primary liver tumors may be due to liver damage from the cirrhosis that was the causative etiology of their liver tumor development. Abnormally high levels of IgG-G0 have additionally been reported in cancers of the pancreas and ovary [20, 21], and as well with increased rates of metastasis in

prostate, gastric, and lung cancers [22, 23]. Our observations show that additional IgG-G0 associations can be found in patients with tumors of the liver, lung and kidney [40]. Interestingly, one of our lung cancer patients, who had by far the largest incidence of IgG-G0, was the only one out of six lung ablation patients who developed metastatic disease (**Table 1**), strengthening the claim that high levels of IgG-G0 may provide some indication for the likelihood of cancer to metastasize. However, care has to be taken when interpreting the findings, as increased IgG-G0 has been known to also reflect general inflammatory conditions, which may be altered during tumor development and metastasis [41].

We also noted higher levels of asialylated IgG (S0) that mimicked the higher levels of agalactosylated IgG in liver tumor patients. Both liver and lung tumor patients presented higher levels of sialylation of galactosylated glycans than controls. As such, the lower levels of monosialylated IgG glycans observed in liver tumor patients are likely due to the lower levels of galactosylated glycans.

We were unable to come up with conclusive results regarding either change in fucosylation following ablation or differing levels of fucosylation amongst different cancer groups. Previous research has indicated that fucosylation is one of the most potent factors of IgG glycosylation. The removal of the core fucose residue has been noted to cause an increased interaction of IgG with FcγRIIIa resulting in a more than 50-fold increase in tumor-destructive ADCC activity (42).

One of the most important findings coming from this study was the differentiation that we noted between patients with clear cell RCC tumors compared to papillary RCC tumors. Our data showed significantly lower rates of sialylation in clear cell RCC patients compared to papillary RCC patients and our control group. Identifying differences in glycosylation between IgG of two different pathologies of renal cancer is an important step in understanding how each of these pathologies manifest. Furthermore, this may help discover methods of treatment and resistance to disease progression, and unveiling pathology-specific biomarkers. This knowledge of differing glycosylation patterns could play a large role in a diagnosis algorithm for RCC, such as has already been explored for ovarian cancer [21]. Clear cell RCC tumors are more common, comprising 80% or renal cell cancers. Typically, they are

hypervascular, more aggressive and are associated with a worse prognosis compared to papillary RCC [40]. A possible explanation to connect these findings is that the higher levels of sialylation that we have seen in papillary RCC patients, with accompanying decrease in inflammation, may contribute to the less aggressive nature of the papillary RCC tumors compared to clear cell RCC.

Correlation analysis between patient clinical outcome and derived IgG glycosylation traits in a model unadjusted for tumor location did show a relationship. However, adjusting for tumor location indicated that this relationship was solely based on associations of glycosylation trait values with specific tumor locations, as the liver patients we enrolled tended to have relatively poor outcomes compared to other ablation groups, as well as distinctive glycosylation characteristics such as high levels of IgG-G0 and IgM-G0. Furthermore, longitudinal analysis of patient IgG and IgM glycosylation through their six-month observation period via linear mixed effects model did not identify any significant patterns of change.

To conclude, this study represents a major area of future investigation in the study of IgG and IgM glycosylation changes after IGTA, and has highlighted several relationships of potential interest. However, additional research with a larger cohort of patients is required in order to further validate these findings.

Acknowledgements:

Research reported in this publication was supported by the National Institute of General Medical Sciences of the National Institutes of Health under award P20GM103421. The previous segment of this project was supported by the National Center for Research Resources (NCRR) under award P20RR017695. This publication was also supported by Program of the European Union FP7 HTP-GlycoMet (contract #324400; authors Josić, Lauc and Andjelković) and the European Union FP7-HighGlycan grants (contract #278535; authors Pučić-Baković, Vučković, Trbojević-Akmačić, Reiding and Wuhrer).

List of references:

1. Ahmed, M., C. L. Brace, F. T. Lee, and S. N. Goldberg. Principles of and advances in percutaneous ablation. Radiology 258 (2011) 351–369. DOI: 10.1148/radiol.10081634

2. Al-Sakere, B., Bernat, C., André, F., Connault, E., Opolon, P., Davalos, R.V., Mir, L.M. A study of the immunological response of tumor ablation with irreversible electrocorporation. Technol. Cancer Res. Treat. 6 (2007) 301-305. DOI: 10.1177/153303460700600406

3. Dupuy, D. E. Image-guided thermal ablation of lung malignancies. Radiology 260 (2011) 633–655. DOI: 10.1148/radiol.11091126

4. Chu, K.F., Dupuy, D.E. Thermal ablation of tumors. Biological mechanism and advances in therapy. Nat. Rev. Cancer 14 (2014) 199-208. DOI: 10.1038/nrc 3672

5. Haen, S. P., P. L. Pereira, H. R. Salih, H.-G. Rammensee, and C. Gouttefangeas. More than just tumor destruction: immunomodulation by thermal ablation of cancer. Clin. Dev. Immunol. 160250 (2011) DOI: 10.1155/2011/160250

6. Kesari, Y., Hochman, I., Confino, H., Korenstein, R., Kelson, I. Activation of local and systematic tumor immune responses by ablation of solid tumors with intratumoral electrochemical or alpha radiation treatments. Cancer Immunol. Immunother. 63 (2014) 1-9. DOI: 10.1007/s00262-013-1462-2

7. Von Mensdorff-Pouilly, S., A. A. Verstraeten, P. Kenemans, F. G. Snijdewint, A. Kok, G. J. Van Kamp, M. A. Paul, P. J. Van Diest, S. Meijer, and J. Hilgers. Survival in early breast cancer patients is favorably influenced by a natural humoral immune response to polymorphic epithelial mucin. J. Clin. Oncol. 18 (2000) 574–583.

8. Formenti, S., Demaria, S. Systematic affects of local radiotherapy. Lancet Oncol. 10 (2009) 718-726. DOI: 10.1016/s1470-2045(09)70082-8

9. Waitz, R., Solomon, S.B., Petre, E.N., Trumble, A.E., Fassò, M., Norton, L., Allison, J.P. Potent induction of tumor immunity by combining tumor cryoablation with anti-CTLA-4 therapy. Cancer Res. 72 (2011) 430-439. DOI: 10.1158/008-5472.CAN-11-1782

10. Sabel, M.S., Arora, A., Su, G. Chang, A.E. Adoptive immunotherapy of breast cancer with lymph node cells primed by cryoablation of the primary tumor. Cryobiol. 53 (2006) 360-366. DOI: 10.1016/j.cryobiol.2006.07.004

11. Ravindranath, M.H., Wood, T.F., Soh, D., Gonzales, A., Muthgounder, S., Perez, C., Morton, D.L., Bilchik, A.J. Cryosurgical ablation of liver tumors in colon cancer patients increases the serum total ganglioside level and then selectively augments antiganglioside IgM. Cryobiol. 45 (2002) 10-21. DOI:10.1016/S0011-2240(02)00102-5

12. Arnold, J. N., M. R. Wormald, R. B. Sim, P. M. Rudd, and R. a Dwek. The impact of glycosylation on the biological function and structure of human immunoglobulins. Annu. Rev. Immunol. 25 (2007) 21–50. DOI: 10.1146/annurev.immunol.25.022106.141702

13. Shields, R. L., A. K. Namenuk, K. Hong, Y. G. Meng, J. Rae, J. Briggs, D. Xie, J. Lai, A. Stadlen, B. Li, J. A. Fox, and L. G. Presta. High resolution mapping of the binding site on human IgG1 for Fc gamma RI, Fc gamma RII, Fc gamma RIII, and FcRn and design of IgG1 variants with improved binding to the Fc gamma R. J. Biol. Chem. 276 (2001) 6591–6604. DOI: 10.1074/jbc.M009483200

14. Malhotra, R., M. R. Wormald, P. M. Rudd, P. B. Fischer, R. A. Dwek, and R. B. Sim. Glycosylation changes of IgG associated with rheumatoid arthritis can activate complement via the mannose-binding protein. Nat. Med. 1 (1995) 237–243.

15. Kaneko, Y., F. Nimmerjahn, and J. V Ravetch. Anti-inflammatory activity of immunoglobulin G resulting from Fc sialylation. Science 313 (2006) 670–673. DOI: 10.1126/science.1129594

16. Anthony, R. M., and J. V Ravetch. A novel role for the IgG Fc glycan: the anti-inflammatory activity of sialylated IgG Fcs. J. Clin. Immunol. 30 (2010) 9-14. Suppl 1: S9–14. DOI: 10.1007/s10875-010-9405-6

17. Bondt, A., Y. Rombouts, M. H. J. Selman, P. J. Hensbergen, K. R. Reiding, J. M. W. Hazes, R. J. E. M. Dolhain, and M. Wuhrer. IgG Fab glycosylation analysis using a new mass spectrometric high-throughput profiling method reveals pregnancy-associated changes. Mol. Cell. Proteomics 31 (2014) 1–30. DOI: 10.1074/mcp.M114.039537

18. Bondt, A., M. H. J. Selman, A. M. Deelder, J. M. W. Hazes, S. P. Willemsen, M. Wuhrer, and R. J. E. M. Dolhain. Association between galactosylation of immunoglobulin G and improvement of rheumatoid arthritis during pregnancy is independent of sialylation. J. Proteome Res. 12 (2013) 4522–4531. DOI: 10.1021/pr400589m

19. Mehta, A. S., R. E. Long, M. A. Comunale, M. Wang, L. Rodemich, J. Krakover, R. Philip, J. A. Marrero, R. a Dwek, and T. M. Block. Increased levels of galactose-deficient anti-Gal immunoglobulin G in the sera of hepatitis C virus-infected individuals with fibrosis and cirrhosis. J. Virol. 82 (2008) 1259–1270. DOI: 10.1128/JVI.01600-07

20. Chen, G., H. Li, L. Qiu, X. Qin, H. Liu, and Z. Li. Change of fucosylated IgG2 Fc-glycoforms in pancreatitis and pancreatic adenocarcinoma: a promising disease-classification model. Anal. Bioanal. Chem. 406 (2014) 267–273. DOI: 10.1007/s00216-013-7439-3

21. Saldova, R., L. Royle, C. M. Radcliffe, U. M. Abd Hamid, R. Evans, J. N. Arnold, R. E. Banks, R. Hutson, D. J. Harvey, R. Antrobus, S. M. Petrescu, R. a Dwek, and P. M. Rudd. Ovarian cancer is associated with changes in glycosylation in both acute-phase proteins and IgG. Glycobiology 17 (2007) 1344–1356. DOI: 10.1093/glycob/cwm100

22. Kanoh, Y., T. Mashiko, M. Danbara, Y. Takayama, S. Ohtani, S. Egawa, S. Baba, and T. Akahoshi. Changes in serum IgG oligosaccharide chains with prostate cancer progression. Anticancer Res. 24 (2004) 3135–3139.

23. Kanoh, Y., T. Mashiko, M. Danbara, Y. Takayama, S. Ohtani, T. Imasaki, T. Abe, and T. Akahoshi. Analysis of the oligosaccharide chain of human serum immunoglobulin g in

patients with localized or metastatic cancer. Oncology 66 (2004) 365–370. DOI: 10.1159/000079484

24. Breen, L., L. Cao, K. Eom, M. Srajer Gajdosik, L. Camara, J. Giacometti, D. E. Dupuy, and D. Josic. High-throughput fractionation of human plasma for fast enrichment of low- and high-abundance proteins. Blood Transfus. 10 (2012) 89-100. Suppl 2: S89–100. DOI: 10.2450/2012.013S

25. Menni, C., T. Keser, M. Mangino, J. T. Bell, I. Erte, I. Akmačić, F. Vučković, M. Pučić Baković, O. Gornik, M. I. McCarthy, V. Zoldoš, T. D. Spector, G. Lauc, and A. M. Valdes. Glycosylation of immunoglobulin g: role of genetic and epigenetic influences. PLoS One 8 (2013) e82558. DOI: 10.1371/journal.pone.0082558

26. Pučić, M., A. Knežević, J. Vidič, B. Adamczyk, M. Novokmet, O. Polašek, O. Gornik, S. Šupraha-Goreta, M. R. Wormald, I. Redžić, H. Campbell, A. Wright, N. D. Hastie, J. F. Wilson, I. Rudan, M. Wuhrer, P. M. Rudd, D. Josić, and G. Lauc. High Throughput Isolation and Glycosylation Analysis of IgG-Variability and Heritability of the IgG Glycome in Three Isolated Human Populations. Mol. Cell. Proteomics 10 (2011) M111 010090. DOI: 10.1074/mcp.M111.010090

27. Ceroni, A., K. Maass, H. Geyer, R. Geyer, A. Dell, and S. M. Haslam. GlycoWorkbench: A tool for the computer-assisted annotation of mass spectra of glycans. J. Proteome Res. 7 (2008) 1650–1659. DOI: 10.1021/pr7008252

28. Colucci, M., H. Stöckmann, A. Butera, A. Masotti, A. Baldassarre, E. Giorda, S. Petrini, P. M. Rudd, R. Sitia, F. Emma, and M. Vivarelli. Sialylation of N-linked glycans influences the immunomodulatory effects of IgM on T cells. J. Immunol. 194 (2015) 151–157. DOI: 10.4049/jimmunol.1402025

29. Kaveri, S. V, G. J. Silverman, and J. Bayry. Natural IgM in immune equilibrium and harnessing their therapeutic potential. J. Immunol. 188 (2012) 939–945. DOI: 10.4049/jimmunol.1102107

30. Josić, Dj., Andjelković, U., Breen, L., Dupuy, D., Lauc, G., Pučić Baković, M., Vidič, J. High-throughput analysis of plasma samples and determination of changes in glycomic patterns in the immunoglobulins in patients after image-guided tumor ablation. Glycoconj. J. 32 (2015) 220-221. DOI: 10.1007/s10719-015-9596-4

31. Sondermann, P., A. Pincetic, J. Maamary, K. Lammens, and J. V Ravetch. General mechanism for modulating immunoglobulin effector function. Proc. Natl. Acad. Sci. U. S. A. 110 (2013) 9868–9872. DOI: 10.1073/pnas.1307864110

32. Kotlan, B., Stroncek, D., Marincola, F. Intravenous immunoglobulin-based immunotherapy: an arsenal of possibilities for patients and science. Immunotherapy 1 (2009) 995-1015. DOI: 10.2217/imt.09.67

33. Ehrenstein, M. R., and C. A. Notley. The importance of natural IgM: scavenger, protector and regulator. Nat. Rev. Immunol. 10 (2010) 778–786. DOI: 10.1038/nri2849

34. Arnold, J. N. Human Serum IgM Glycosylation: Identification of glycoforms that can bind to mannan-binding lectin. J. Biol. Chem. 280 (2005) 29080–29087. DOI: 10.1074/jbc.M504528200

35. Lissner, R., W. G. Struff, I. B. Autenrieth, B. G. Woodcock, and H. Karch. Efficacy and potential clinical applications of Pentaglobin, an IgM-enriched immunoglobulin concentrate suitable for intravenous infusion. Eur. J. Surg. Suppl. 584 (1999) 17–25. DOI: 10.1080/11024159950188493

36. Rieben, R., A. Roos, Y. Muizert, C. Tinguely, A. F. Gerritsen, and M. R. Daha. Immunoglobulin M-enriched human intravenous immunoglobulin prevents complement activation in vitro and in vivo in a rat model of acute inflammation. Blood 93 (1999) 942–951.

37. Nimmerjahn, F., and J. V Ravetch. The antiinflammatory activity of IgG: the intravenous IgG paradox. J. Exp. Med. 204 (2007) 11–15. DOI: 10.1084/jem.20061788

38. Cavazzuti, I., G. Serafini, S. Busani, L. Rinaldi, E. Biagioni, M. Buoncristiano, and M. Girardis. Early therapy with IgM-enriched polyclonal immunoglobulin in patients with septic shock. Intensive Care Med. 40 (2014) 1888–1896.

39. Grönwall, C., and G. J. Silverman. Natural IgM: beneficial autoantibodies for the control of inflammatory and autoimmune disease. J. Clin. Immunol. 34 (2014) 12-21. Suppl 1: S12–21. DOI: 10.1007/s10875-014-0025-4

40. Iida, S., H. Misaka, M. Inoue, M. Shibata, R. Nakano, N. Yamane-Ohnuki, M. Wakitani, K. Yano, K. Shitara, M. Satoh. Nonfucosylated therapeutic IgG1 antibody can evade the inhibitory effect of serum immunoglobulin G on antibody-dependent cellular cytotoxicity through its high binding to FcgammaRIIIa. Clin. Cancer Res. 12 (2006) 2879–2887. DOI: 0.1158/1078-0432.CCR-05-2619

41. Dall'Olio, Vanhooren, V., Chen, C. C., Slagboom, P. E., Wuhrer, M., Francheschi, C. N-glycomic biomarkers of biological aging and longevity: A link with Inflammaging. Ageing Res. Rev. 12 (2013) 685-698.

42. Ficarra V, Brunelli M, Cheng L, Kirkali Z, Lopez-Beltran A, Martignoni G, Montironi R, Novara G, Van Poppel H. Prognostic and therapeutic impact of the histopathologic definition of parenchymal epithelial renal tumors. Eur. Urol. 58 (2010) 655–668. DOI: 10.1016/j.eururo.2010.08.001

Figure legends:

Figure 1. Representative example of a chromatogram obtained by HILIC-UPLC analysis of IgG N-glycans of a healthy person. Only the most abundant N-glycans in each chromatography peak are shown. For a full list of detected IgG N-glycans see Supplementary Table 1. Glycan schemes are given in terms of: square (N-acetylglucosamine), triangle (fucose), dark circle (mannose), light circle (galactose), and diamond (N-acetylneuraminic acid).

Figure 2. Representative example of a chromatogram obtained by HILIC-UPLC analysis of IgM N-glycans. Only the most abundant N-glycans in each chromatography peak are shown. For a full list of detected IgM N-glycans see Supplementary Table 2. Glycan schemes are given as in Figure 1.

Figure 3. Comparison of derived IgG glycosylation traits of controls and tumor (liver, lung and renal) patients before ablation. G0 – the prevalence of agalactosylated glycans, G2 - the prevalence of digalactosylated glycans, F – the prevalence of core-fucosylated glycans, B - the prevalence of glycans with bisecting *N*-acetylglucosamine, and S1 – the prevalence of monosialylated glycans. Standardized values of derived glycosylation traits on y-axis.

Figure 4. Comparison of derived IgM glycosylation traits of controls and tumor (liver, lung and renal) patients before ablation. Description of derived glycosylation traits as in Table 2. Standardized values of derived glycosylation traits on y-axis.

Figure 5. IgG N-glycan profile of renal tumor patient with unexpectedly high abundant oligomannose N-glycans.